Tellus (1989), *41A*, 32–47

Simulation of sea surface temperatures with the surface heat fluxes from an atmospheric circulation model

By MEHMET KARACA, *Climate Dynamics Laboratory and Department of Atmospheric Sciences, University of California, Los Angeles, CA 90024, USA* and DETLEV MÜLLER, *Climate Dynamics Laboratory and Institute of Geophysics and Planetary Physics, University of California, Los Angeles, CA 90024, USA*

(Manuscript received 15 June 1987; in final form 3 May 1988)

ABSTRACT

The global fields of the surface heat fluxes for the December–February period are calculated with the UCLA atmospheric circulation model (ACM). This model operates on a global grid net. The planetary boundary layer (PBL), as the decisive subsystem for the surface fluxes, is parameterized in terms of its bulk properties. For several locations in the north Atlantic, the model heat fluxes are incorporated into the forcing of a simple ocean mixed-layer (OML) model. The OML-model uses a slight generalization of the bulk Kraus-Turner concepts incorporating thermocline contributions to the buoyancy budget of the upper ocean. The remaining components of the OML-forcing are estimated from weather-ship data. The comparison of the sea-surface temperatures (SST), prescribed to the ACM as lower boundary condition, with those obtained from the OML model-integration provides a consistency test for the ACM-fluxes.

1. Introduction

The heat fluxes at the earth's surface provide a major link between the atmosphere and the slower components of the terrestrial climate system, namely the oceans, the cryo- and the biosphere. Variations of these fluxes are not only related to phenomena as elementary as the seasonal signal. In general, they expose the high degree of complexity characterizing the entire coupled system. Currently, the particular role of the surface heat fluxes (and wind-stresses) in the ocean-atmosphere system is extensively discussed in view of the "El Niño-Southern Oscillation" phenomenon.

Physically the surface fluxes are determined by radiative and turbulent processes in the PBL and the upper ocean, which in turn are strongly affected by dynamic and thermodynamic processes in the free atmosphere and the deep ocean, respectively. Hence, the most adequate modelling strategy with respect to the air-sea interaction employs coupled experiments with atmospheric and oceanic circulation models (Manabe et al., 1975). The experiments considered in the present paper utilize a simpler model design. Here, the surface heat fluxes will be obtained from an integration of the UCLA atmospheric circulation model with prescribed SST fields. These fluxes will then be incorporated into the forcing of a simple, 1-dimensional OML-model, which in turn yields the SST and heat capacity of the upper ocean. Regarding the physics of the air-sea interaction this type of experiment exhibits some limitations. In contrast to a coupled ocean-atmosphere model, the ACM is integrated independently from the OML with prescribed SST. The optimal result of the OML-integration can thus only be a verification of these boundary conditions. If, however, this can be achieved, the experiment provides a relevant consistency test for the model heat fluxes. Secondly, a bulk mixed layer model is a poor representation of the ocean dynamics on a seasonal time-scale. Though these models capture the major aspects of the dynamics of the vertical buoyancy structure of the upper ocean, they do not cover dynamically the contributions of large scale advection and turbulent horizontal diffusion to the buoyancy budget of the upper ocean at a given location. In the paper at hand, the latter effects will be estimated from data.

Directly involved in the air-sea interaction are only the PBL and the ocean mixed-layer, both of which are dominated by turbulent mixing and entrainment processes. Turbulence theory is presently not able to provide a detailed description of these systems. Hence the models considered in the present paper employ bulk, but nevertheless sufficiently flexible concepts, which circumvent the problems of turbulence theory.

The bulk PBL-parameterization used in the UCLA-ACM goes back to Deardorff (1972). Particular problems arise in the atmosphere from the occurrence of water-phase transformations. A formulation of cumulus convection that is compatible with the PBL-model has been given by Arakawa and Schubert (1974), while stratocumulus clouds have been implemented by Randall (1979). Surface fluxes can then be expressed in terms of the bulk properties of the PBL and the conditions at the lower boundary. The global fields of the surface heat fluxes for the December to February season have been calculated in several ACM runs. While all of these runs use the same boundary condition, they start from slightly different initial conditions. The climatological features of the heat fluxes obtained from these experiments will be discussed in detail in section 2. Similar results for the (spectral) ACM of the ECMWF have been published by Simonot (1986) and currently available observations for the ocean regions of the globe's surface are provided by the atlas of Esbensen and Kushnir (1981).

The bulk approach to turbulent mixing and entrainment processes in the upper ocean has been introduced by Kraus and Turner (1967). Heat transfer across the mixed-layer base and turbulent diffusion in the layer beneath (the thermocline) are then generally modelled in terms of a diffusion equation. Models of this type hence require the introduction of a vertical grid beneath the mixed-layer and an estimate of the magnitude of the turbulent diffusion coefficient (Denman and Miyake, 1973). Since such estimates are notoriously questionable, turbulent transport coefficients play in practice the role of more or less free tuning parameters.

In the present paper, an alternative model-version will be utilized. According to Hasselmann (Maier-Reimer et al., 1982) the turbulent velocity field in the upper ocean establishes essentially a characteristic temperature profile that remains self-similar and can be described in terms of a few profile parameters. With appropriate "closure-assumptions" the Kraus-Turner budgets can be generalized to include thermocline processes. This approach is computationally much more effective than the Kraus-Turner budgets in conjunction with a partial differential equation. Moreover the particular "closure" employed here does not invoke additional model parameters, which could be subject to numerical tuning. Details of the model and a comparison to ocean data will be given in section 3.

Besides the atmospheric heat fluxes, a SST simulation in terms of a mixed layer model requires the knowledge of the advective heat flux and the time rate of change of turbulent kinetic energy (TKE) in the upper ocean at the location under consideration. In the present paper, these forcing components will be estimated from data. The data at hand (kindly provided by the British Meteorological Office) were time series of temperature profiles of the upper ocean at 6 North Atlantic weathership locations. These data do not contain direct information about advective fluxes or the time rate of change of TKE. They do yield, however, the total heat content and the total potential energy in the oceanic column at each instant. Conversely, these parameters admit conclusions on the corresponding fluxes. The SST simulation will then be performed at the 6 weathership locations, where the complete forcing can be obtained as an appropriate combination of the ACM results and those fluxes derived from the data. The OML-integration and the comparison of the model SST and the ACM boundary conditions will be discussed in Section 4.

2. The model heat fluxes

The UCLA-ACM is formulated in terms of the primitive equations utilizing prescribed pressure levels as coordinate surfaces above the PBL. Present results have been obtained with the coarse version of the model, employing a horizontal 4° × 5° grid and 9 layers in the vertical at a time-step of 7.5 min. The model covers diurnal and seasonal cycles. Its prognostic variables are potential temperature, ground temperature over land, surface pressure, the mixing ratios of water vapor and ozone, the PBL-depth and the horizontal velocities. An extensive model description may be found elsewhere (Arakawa (1972); for a more recent update see for instance Suarez et al., (1983).

Heat fluxes have been evaluated from 6 ACM runs under the same boundary conditions, starting however from different initial conditions. At the surface, monthly means of the climatological SST-field as well as the sea ice boundary are prescribed as lower boundary condition. Initial conditions were chosen for several dates at the beginning of October, corresponding to the years 1979 and 1982, respectively. The following results correspond to the December–February period of these runs.

The net surface heat fluxes

$$F_q(t,\mathrm{ACM}) = \mathrm{SRAD} - \mathrm{LRAD} - \mathrm{LATF} - \mathrm{SENF}$$

are composed of the solar (SRAD) and the terrestrial (LRAD) radiative as well as the latent (LATF) and sensible (SENF) fluxes of heat. The parameterization for the radiative fluxes are due to Katayama (1972) and Schlesinger (1976). These authors treat the problem of cloud cover by assuming overcast conditions at a given gridpoint, if the relative humidity exceeds saturation, a stratocumulus layer is present in the PBL or cumulus clouds extend above the 500 mb level. Under cloudless conditions, solar radiation is only depleted by absorption due to water vapor or Rayleigh scattering. Longwave radiation is considered isotropic and multiple reflections are ignored.

The turbulent fluxes LATF and SENF are parameterized according to Deardorff (1972) in terms of surface conditions and the bulk PBL properties. Employing similarity arguments, the relation of the surface fluxes and the profiles of temperature, moisture and wind in the lower atmosphere can be formulated in terms of the ratio of the PBL depth to the Monin-Obukov length. A detailed, recent review of these flux parameterizations can be found in Suarez et al. (1983). It should be mentioned that the contribution of precipitation to the latent heat flux will be ignored in the following in view of the air-sea interaction. Precipitation plays an important rôle for the dynamics of the PBL, where the phase transition actually takes place. In the ocean, on the other hand, this contribution would be felt as $P = c_p(T_a - T_s)$, where c_p denotes the heat capacity and T_s the temperature of sea-water, while T_a is the temperature of the raindrop (assumed to be air-temperature). This term is always orders of magnitude smaller than the evaporative term.

The ACM provides the radiative fluxes every 5 days and the turbulent fluxes every 12 hours. The basic data set referred to in the following consists of 10-day means of these model results, averaged furthermore over all 6 runs. The entire 3-month period from December to February is thus covered by a time-series of 9 global maps for each of the flux components as well as the net flux.

Monthly means of the net fluxes F_{ACM} are shown in Fig. 1 Comparison of these results with the observations of Esbensen and Kushnir (1981) shows a high degree of coincidence among the corresponding patterns. The model produces a well-pronounced summer-winter contrast between the two hemispheres, inasmuch as the atmosphere heats the oceans in the summer-hemisphere, while the net flux has the opposite sign over the northern oceans. Furthermore, the model clearly exhibits large fluxes over the warm western boundary current in the northern hemisphere. Additional extrema are noted over the Norwegian Sea and the Aleutians, where the open ocean is much warmer than the (sub-) polar winter atmosphere. In the southern hemisphere, large fluxes occur over the cold eastern boundary currents. Qualitatively, the entire pattern does not change much in the course of the season.

The most obvious discrepancy with respect to the net flux data of Esbensen/Kushnir are the pronounced extrema west of Mexico and Indochina. These will be discussed below. As far as numerical values are concerned, the model results display the tendency to exceed Esbensen and Kushnir's data by a factor of order 1.5.

Fig. 2 shows monthly means of the individual components of the net flux for January. Besides the expected zonal structure, the short-wave radiation (Fig. 2a) reflects essentially the para-

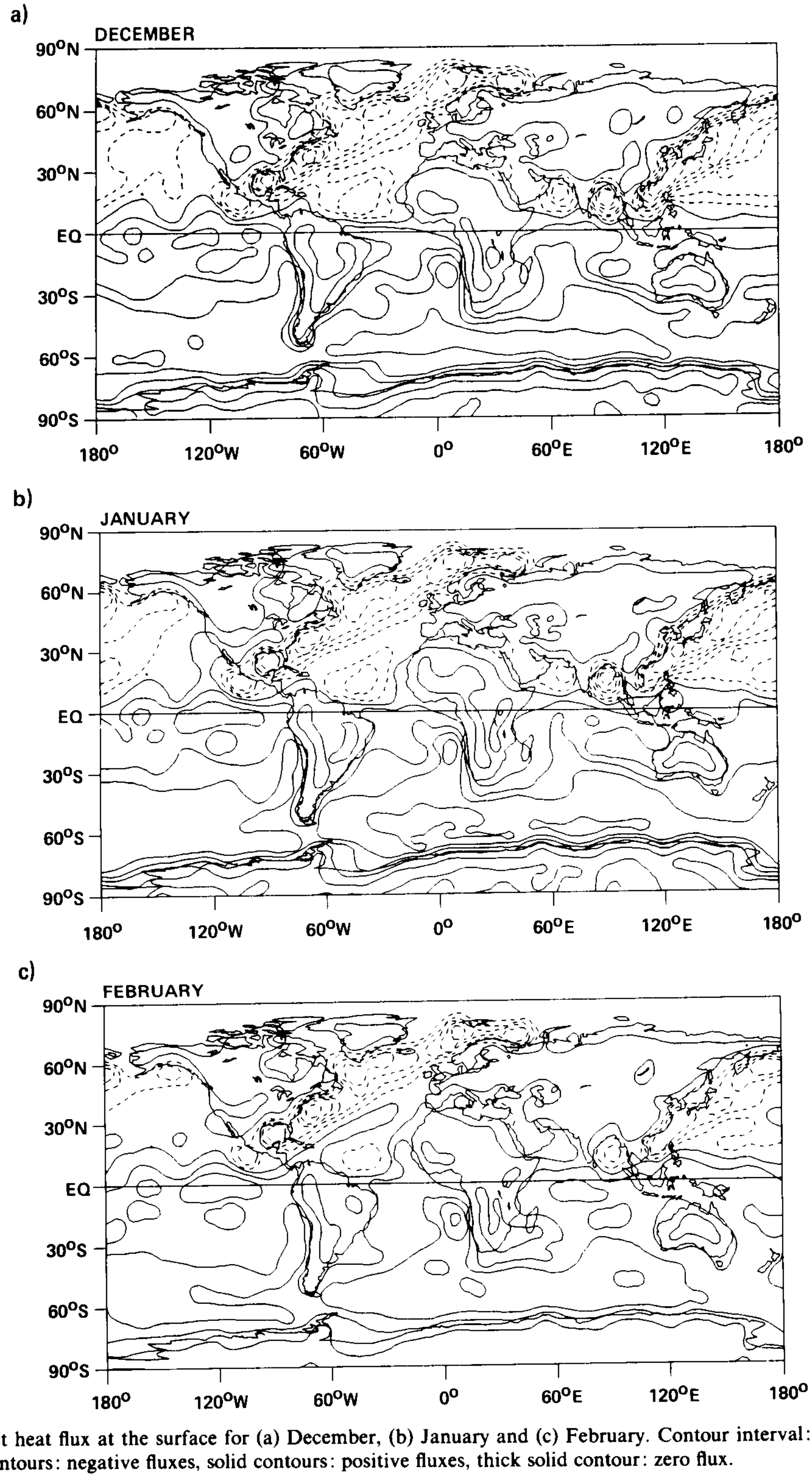

Fig. 1. Net heat flux at the surface for (a) December, (b) January and (c) February. Contour interval: 75 W/m^2. Dashed contours: negative fluxes, solid contours: positive fluxes, thick solid contour: zero flux.

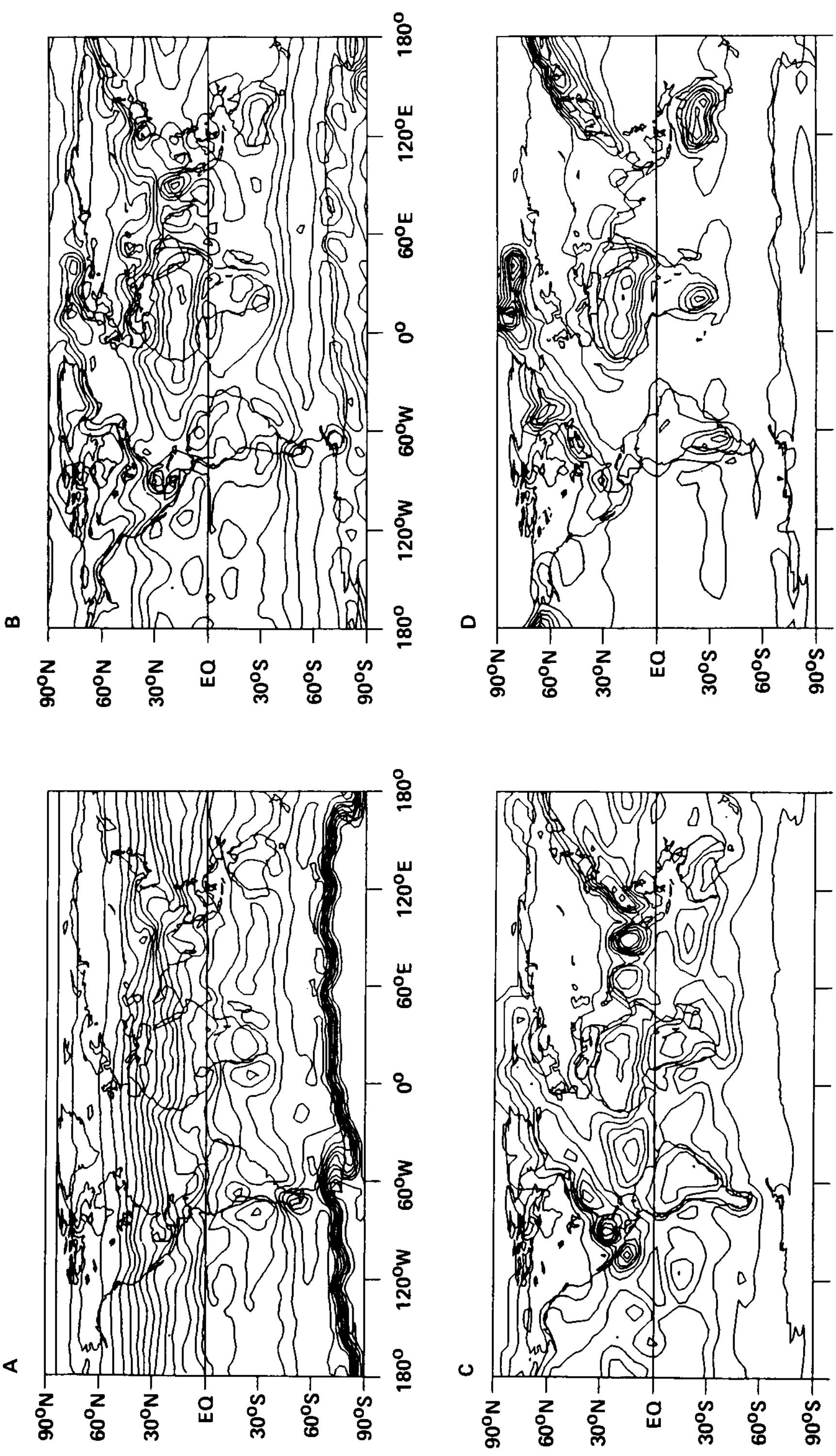

Fig. 2. Heat flux components at the surface for January: (a) solar radiation SRAD; (b) long-wave radiation LRAD; (c) latent heat flux (evaporation) LATF; (d) sensible heat flux SENF.

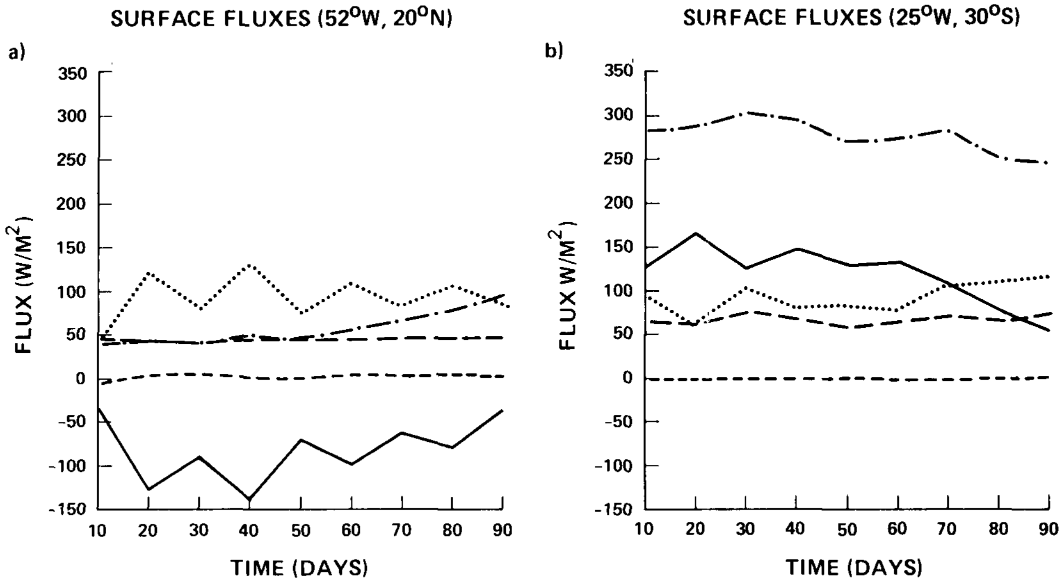

Fig. 3. Seasonal course of surface fluxes at (a) 52°W, 20°N (north Atlantic; (b) 25°W, 30°S (south Atlantic). Dotted line: LATF, short dashed line: SENF, long dashed line: LRAD, dot dashed line: SRAD, solid line: net flux.

meterization of the surface-albedo. Particularly, north of Antarctica the fairly sharp transition from open sea water with an albedo of order 0.2 to snow covered land ice with an albedo of order 0.6 can be well observed.

The long-wave radiation (Fig. 2b) does not display significant differences with the data of Esbensen and Kushnir or with the results of the ECMWF-model (Simonot, 1986).

The latent heat flux (Fig. 2c) clearly shows that evaporation is mainly responsible for the large fluxes west of Mexico and Indochina, already observed in Fig. 1. Obviously the model sees here a pronounced flow of dry air moving over the corresponding continents towards the southwestern coasts. Once this air reaches the ocean, it picks up large amounts of moisture. The physical relevance of this process is also suggested by the latent heat flux data of Esbensen and Kushnir, which do show large evaporation over these areas. However, due to the coarse horizontal resolution and the ignorance of turbulent diffusion, the ACM may quantitatively overestimate this effect.

The sensible heat flux (Fig. 2d) is seen to be large over the western boundary currents and the open (sub-) polar oceans of the northern hemisphere. This coincides with the corresponding picture of Esbensen and Kushnir. Over the continents, where the Esbensen and Kushnir-atlas does not provide data, the ACM exhibits extreme heat fluxes over the globe's desert regions.

Fig. 3 shows the seasonal course of the fluxes in terms of time-series of model results for 2 fixed ocean locations. In the northern hemisphere (Fig. 3a) the 4 flux components are typically of comparable magnitude and the net flux is negative, increasing towards the end of winter. In the southern-hemisphere (Fig. 3b) the solar radiation is significantly larger than the other components and the net flux. In both cases the latent heat flux is seen to exhibit the largest variance.

The climatological features of the surface heat flux fields calculated by the UCLA-ACM basically coincide with the observations of Esbensen and Kushnir as well as with corresponding results from the ECMWF-model. Large variations occur in the results of the UCLA-model of the latent heat flux due to its strong dependence on small scale processes. A detailed analysis of the quantitative differences between the 3 data sets would have to be performed in terms of statistical significance test. This is not subject of the present paper.

3. The ocean mixed-layer-model

Atmospheric heat fluxes together with the heat, advected by the surrounding oceans decisively determine the SST at a given location. It is, however, the characteristic problem of SST-dynamics that the effective heat capacity of the upper ocean, i.e., essentially the ML-depth, is subject to temporal variations. This variability is due to turbulent mixing processes at the air-sea interface and within the ML as well as entrainment at and vertical heat transfer across the ML-base. SST dynamics thus depend on the dynamics of the entire vertical buoyancy structure of the upper ocean. OML-models of the Kraus-Turner type provide a bulk phenomenological description of this system. The following data inspection suggests a slight modification of the original Kraus-Turner concepts to include the contribution of thermocline processes to the buoyancy-budget of the upper ocean.

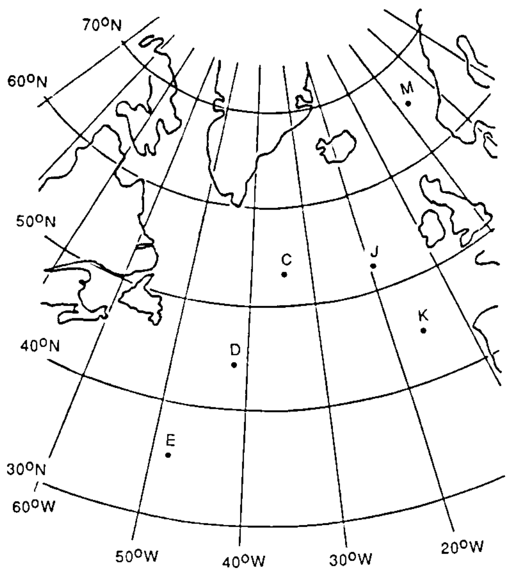

Fig. 4. Weathership locations in the north Atlantic.

The data at hand are time-series of bathythermograph temperature-profiles $T(t, -275\ \mathrm{m} \leqslant z \leqslant 0\ \mathrm{m})$ at 6 north Atlantic weathership locations, shown in Fig. 4. It should be mentioned that the weathership locations do not coincide with grid-points of the ACM. ACM results, to be applied at these locations later, will thus be linearly interpolated from the generally 4 surrounding grid-points.

Each of these profiles represents a 5-day mean and the total time-series cover a period of about 8 years per ship. Some characteristics of the original data-set are given in Table 1 and for weathership E these data are shown in Fig. 5. From the original data a mean seasonal cycle of 73 profiles was constructed for each ship by averaging over all years for a given phase of the year. This data-processing eliminates data gaps and yields a climatological picture of the seasonal cycle in the upper ocean. For weathership J this average year is shown in Fig. 6. Qualitatively the same pictures are obtained at the other weatherships.

Table 1. *Statistics of weathership-data*

WS	LAT	LON	LTS	NCOM	INC	MIS	INITP	FINP
C	53°N	35°W	596	425	108	63	13 Oct 1965	11 Dec 1973
D	44°N	41°W	565	372	123	70	28 Sep 1965	24 Jun 1973
E	35°N	48°W	566	411	74	81	28 Sep 1965	29 Jun 1973
J	52°N	20°W	694	527	118	49	28 Sep 1965	31 Mar 1975
K	45°N	16°W	694	458	110	126	28 Sep 1965	31 Mar 1975
M	66°N	2°E	639	499	35	105	30 Sep 1965	31 Mar 1975

WS: weathership. LAT: latitude. LON: longitude. LTS: Length of time-series. NCOM: complete profiles. INC: incomplete profiles. MIS: missing profiles. INITP: date of initial profile. FINP: data of final profile.

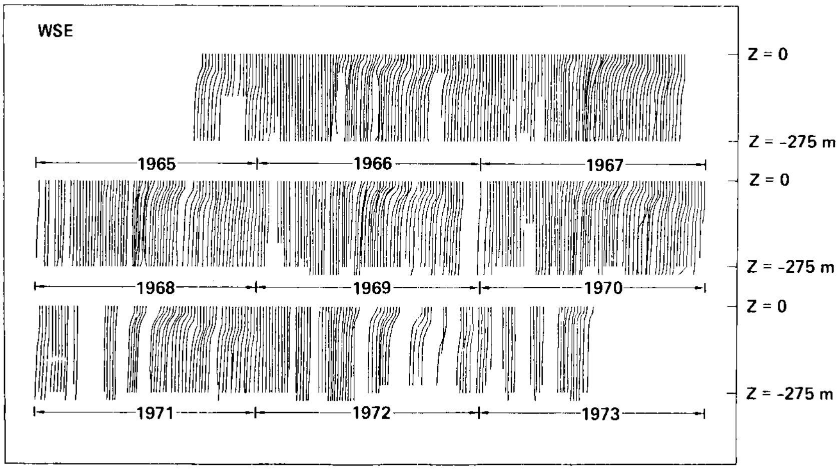

Fig. 5. Original temperature data at weathership E. The vertical scale corresponds to $z = 0$ at the surface down to $z = -300$ m for the longest profiles.

For all ships considered, the temperature-data provide sufficient information on the buoyancy-structure of the upper ocean, i.e. salinity does not affect the situation significantly. In water with a low salt content, this conclusion can be drawn from temperature-data alone due to fundamental stability-requirements. Stability of the column requires buoyant water always to lie above less buoyant water. With respect to stability, buoyancy is thus sufficiently represented by temperature alone, if the temperature does not increase downwards. At the above locations, this is always the case. However, in very high latitudes beneath the polar sea-ice cover, this situation changes basically (Lemke and Manley, 1984): in this region the buoyancy structure of the upper ocean is dominated by salinity effects. But even at some locations in the open ocean, salinity cannot be ignored. From a time-series of temperature-profiles this is evident, if a significantly large fraction of the profiles exhibits a temperature-increase downwards. In these cases, it has to be concluded that the column is stable, since otherwise these profiles would not be observed at a significant rate. But, as temperature does not ensure stability, salinity contributions must be relevant. This was the case for a time-series from weathership A, located at 62°N and 33°W, where about 20% of the profiles were "thermally unstable". Due to the lack of salinity data, this time-series was discarded from the following considerations.

Fig. 6 displays several system parameters, which are readily derived from the data without further assumptions (solid lines). These are the bottom temperature

$$T_b := T(t, z = -h_2),$$

where $h_2 = 275$ m. Furthermore the sea-surface temperature

$$T_s(t) := T(t, z = 0 \text{ m})$$

and the zeroth and first moment of the temperature distribution with respect to the bottom temperature

$$S_\nu(t) := \int_{-h_2}^{0} dz(T(t,z) - T_b)\,(-z)^\nu, \quad \nu = 0,1 \quad (3.1a)$$

where the sign in the first moment has merely been introduced for computational convenience.

Kraus-Turner models assign now these moments with a simple physical meaning by assuming the familiar linear relationship between the density of gravitational charge ρ and temperature for sea water

$$\rho = \rho_0[1 - \alpha(T - T_0)] \quad (3.2)$$

where ρ_0 is the constant density of inertia, T_0 some appropriately chosen reference temperature and $\alpha = O(10^{-4}/K)$ the small and constant coefficient of thermal expansion for sea-water. (3.2) ignores salinity-effects, which are irrelevant for the present purposes, as mentioned earlier. The incorporation of salinity-effects into Kraus-

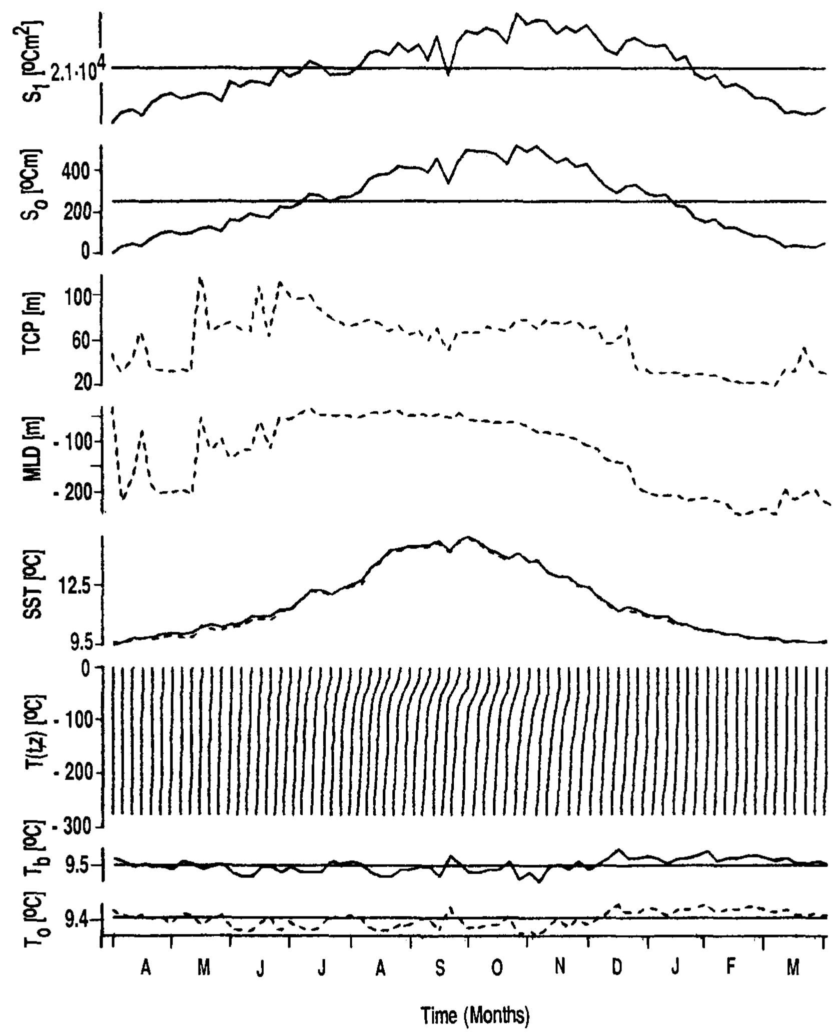

Fig. 6. Seasonal cycle of temperature profiles, profile-parameters and profile-moments at weathership J. The first profile corresponds to 24 March. MLD: mixed-layer depth h_1; TCP: thermocline-parameter h_{12}. See text for further details.

Turner type models is straightforward and has been extensively discussed for instance by Lemke and Manley (1984).

With this relation, the total mass of the column has to be taken as

$$M = \int_{-h_2}^{0} \mathrm{d}z \rho_0 = \rho_0 h_2$$

and the conservation of mass

$$\dot{M} = \dot{M}_1 + \dot{M}_2 = 0,$$

where $M_1 = \rho_0 h_1$ denotes the mass of the mixed layer of depth h_1 and $M_2 = \rho_0(h_2 - h_1)$ the mass of the thermocline, simply states that the system is thermodynamically closed and made up by 2 open subsystems, exchanging matter by entrainment. Though advection will not be considered in this paper, it may be noticed that this statement is equivalent to the kinematic boundary conditions that the sea-surface (and the system bottom) be material surfaces, while the mixed-layer base at $z = -h_1$ is not.

With (3.2) the first moments of the temperature distribution can now be associated with the total buoyancy, defined as the negative weight of the column, and the potential energy of the system. Introducing the moments with respect to the reference temperature T_0

$$R_\nu := S_\nu + \frac{1}{\mu} T_{20} h_2^\mu \quad \nu =: \mu - 1 = 0,1 \tag{3.1b}$$

where $T_{20} := T_b - T_0$ one obtains for the buoyancy

$$B = -g \int_{-h_2}^{0} \mathrm{d}z\rho = \alpha g \rho_0 R_0 - Mg. \tag{3.3}$$

Since on the other hand the total content of the system is given as

$$Q = c_p \rho_0 \int_{-h_2}^{0} \mathrm{d}zT = c_p \rho_0 R_0 + c_p M T_0 \tag{3.3a}$$

buoyancy measures essentially the system's heat content according to

$$B = \frac{\alpha g}{c_p} Q - B_0,$$

where $B_0 := g(1 + \alpha T_0)M = \text{const.}$ Potential energy is defined in this framework as

$$E_p := -Bz_0,$$

where

$$z_0 := (B_1 z_1 + B_2 z_2)/B$$

is the center of gravity of the total column, while z_n and B_n denote the gravity centers and buoyancy contents of the 2 subsystems. With (3.2), the potential energy may now also be written as

$$E_p = g \int_{-h_2}^{0} \mathrm{d}z\rho z = \alpha g \rho_0 R_1 - \tfrac{1}{2} Mgh_2. \tag{3.4}$$

It follows from (3.3) and (3.4) that the time-series for S_0 and S_1, shown in Fig. 6, essentially reflect the seasonal course of the heat content and the center of gravity in the upper ocean. Note that the maximum in heat precedes the maximum of potential energy by 2 weeks or so, as already observed at weathership E by Gill and Turner (1976). This phase shift clearly indicates a nontrivial relation between the heat capacity of the upper ocean and the depth of its center of gravity.

With these definitions, Fig. 6 suggests the following phenomenology for the course of the season in the upper ocean. First a comparison of $T_s(t)$ and T_b shows that the latter does not exhibit a signal with relevance to the seasonal time-scale. As it is well known (Oort and Von der Haar, 1976) seasons do not penetrate into the ocean below some 300m. During spring now, a more or less homogeneous water column is supplied with heat from the surface. Turbulent kinetic energy, also generated at the surface, mixes this heat into the ocean such that an upper mixed layer is established. Excess turbulent kinetic energy entrains colder and hence heavier water from below, which in turn leads to the emergence of a sharp buoyancy gradient in the thermocline. During cooling, mixed layer deepening erases the gradient and during autumn and winter the entire system becomes mixed. Finally turbulence dies out and the process starts again with next year's heating period.

According to this picture, TKE mixes buoyant water into the ocean and entrains heavy water into the mixed layer, thus displacing the system's center of gravity. The time rate of change of turbulent kinetic energy F_p, therefore provides the work necessary to change the potential energy of the total column, i.e., from (3.4)

$$F_p = \frac{\mathrm{d}}{\mathrm{d}t} R_1, \tag{3.5a}$$

where the physical constants have been incorporated into F_p. Furthermore, the buoyancy budget of the column is given according to (3.3) and (3.3a) as

$$F_q = \frac{\mathrm{d}}{\mathrm{d}t} R_0, \tag{3.5b}$$

where F_q denotes the total heat flux into the system and physical constants have again been incorporated into F_q. Notice that in this framework mass (inertia) is conserved, while weight (buoyancy) is not.

It is seen from Fig. 5 or 6 that the turbulent velocity field essentially establishes and maintains a characteristic temperature profile in the upper ocean, which changes quantitatively but not qualitatively in the course of the seasons. This observation has been utilized by Hasselmann (Maier-Reimer et al., 1982) to describe the buoyancy structure of the upper ocean in terms of a temperature profile that remains self-similar in the course of the year. The dynamics of the vertical buoyancy structure of the upper ocean can thus be cast into a low order system of ordinary differential equations for the profile parameters. Following Hasselmann (Maier-Reimer et al., 1982) this profile will here be assumed of the form

$$T(t,z) := \begin{cases} T_1 & 0 \geqslant z \geqslant -h_1 \\ T_0 + T_{10}\,e^D & -h_1 \geqslant z \geqslant -h_2 \end{cases} \tag{3.6}$$

where

$$T_{10} := T_1 - T_0$$

and

$$D(t,z) = (h_1 + z)/h_{12}.$$

One such profile together with the corresponding observation (from ship D) is shown in Fig. 7. Similar models have been used by Lemke and Manley (1984) for the salinity-dominated OML at very high latitudes and by Pollard et al. (1983). In the form (3.6) the model represents phenomenologically complete mixing in the upper-most layer and entrainment at the mixed layer base $z = -h_1(t)$. In addition to the original Kraus-Turner model (1967), this profile also takes account of turbulent conduction beneath the ML

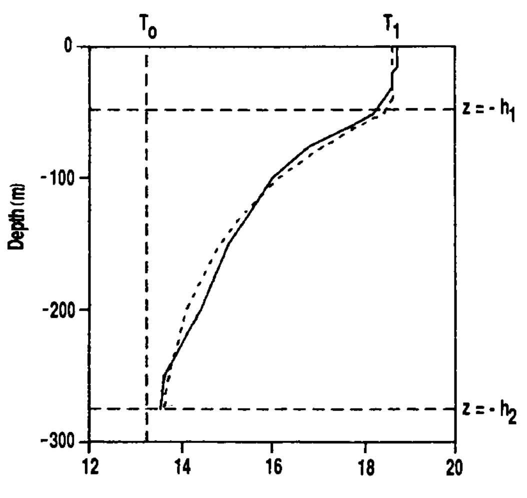

Fig. 7. Observed (solid line) and model-profile (dashed line) for 5 October at weathership D. Profile parameters are: $T_1 = 18{\cdot}6$°C, $T_b = 13.4$°C, $T_0 = 13.2$°C, $h_1 = 47$ m, $h_{12} = 86$ m.

in terms of the exponentially shaped second layer such that the heat content of the thermocline is basically measured in terms of the scale-depth $h_{12}(t)$.

The profile parameters can be empirically determined by means of a least-square fit of (3.6) to the data profiles. As a by-product, this procedure yields a χ^2-test for the statistical significance of the model (3.6). An extended discussion of the statistical techniques involved may be found elsewhere (Müller, 1987). In case of the original dataset, for none of the profiles the model (3.6) had to be rejected at a 95% significance-level. It may be mentioned that the particular shape of the thermocline in (3.6) is actually not crucial, but rather a question of computational convenience. A simple parabola or a Gaussian would exhibit a similar degree of campatibility with the data.

The results of the least-square fit of the profile parameters for the average year at weathership J are shown by the dotted lines in Fig. 6. Similar to the bottom temperature T_b, the asymptotic temperature T_0 does not exhibit a significant signal on this time scale. It will thus be identified with the constant reference temperature, required by (3.2). The mixed-layer temperature $T_1(t)$ (dotted line in the SST-panel of Fig. 6) is basically identical with the SST in the narrow sense $T_S(t)$. Occasionally it is slightly colder than $T_S(t)$ due to minor gradients in the ML itself (see also Fig. 7). The mixed layer depth $h_1(t)$ exhibits typically shallow values of order 20m to 50m for summer and enhanced deepening during autumn and winter. During spring the parameter value $h_1(t)$ fluctuates strongly, since the column does not exhibit major gradients for this time of the year. Consequently the thermocline scale depth $h_{12}(t)$ now also fluctuates strongly. During the rest of the year, $h_{12}(t)$ shows a tendency to decay from values of order 100 m down to values of order 20 m. This corresponds to a tendency to increase for the temperature gradient just below the mixed-layer base

$$\partial_z T(t, z = -h_1) = T_{10}/h_{12},$$

with mixed layer deepening. This is characteristic for the turbulent nature of the entrainment process.

According to (3.1), the profile-moments now read in terms of the profile parameters

$$R_0 = T_{10}h_1 + (T_{10} - T_{20})h_{12}, \tag{3.7a}$$

$$R_1 = \tfrac{1}{2}T_{10}h_1^2 + S_0 h_{12}, \tag{3.7b}$$

and one has the additional relation

$$h_{12} = (h_2 - h_1)/\theta \tag{3.7c}$$

where $\theta := \ell n(T_{10}/T_{20})$. To obtain the complete system dynamics, the Kraus-Turner budgets (3.5) have to be supplemented by a "closure assumption", since so far there are more independent profile-parameters than budget equations. In agreement with the data, it will here be assumed that

$$T_{20} = \text{const.} \tag{3.7d}$$

in the course of the seasons. This assumption is the major difference to the model-versions used by Maier-Reimer et al. (1982) and Lemke and Manley (1984). It has the advantage to avoid the introduction of additional tuning parameters and represents simply the lower boundary condition for the upper ocean. Note that (3.7d) involves 2 temperatures, the reference temperature T_0 and the bottom temperature T_b. But while T_0 plays the role of a universal constant, T_b is characteristic of the level, chosen as system bottom at the given location. Moreover, in the framework of an advective model, T_b may generally be subject to advective transports.

The system is now described in terms of 3 dynamical variables: the ML-temperature $T_{10}(t)$, the ML-depth $h_1(t)$, and the thermocline scale depth $h_{12}(t)$. Due to the self-similarity assumption for the profile these 3 variables are related by the diagnostic relation (3.7c) for all times. Hence, two of these may be arbitrarily chosen to represent the system completely. In the following, the ML-temperature T_{10} and the ML-depth h_1 will be used.

With these assumptions, the Kraus-Turner budgets assume the form

$$F_q = H_q \dot{T}_{10} + (T_{10} - \theta_2)\dot{h}_1 \tag{3.8a}$$

$$F_p = \tfrac{1}{2}H_p F_q + (T_{10} - \theta_2)H_1 \dot{h}_1, \tag{3.8b}$$

where $\theta_2 := (T_{10} - T_{20})/\theta$ and

$$H_q := h_1 + \frac{1}{T_{10}}(T_{10} - \theta_2)h_{12}$$

denotes the effective thermal depth (heat capacity) of the total system while

$$H_p := \tfrac{1}{2}h_1 + (H_q - h_1)H_1/h_1$$

is the gravitational depth of the column with

$$H_q H_1 := \tfrac{1}{2}h_1^2 + [1 - (\theta_2 - T_{20})/(T_{10} - \theta_2)]h_1 h_{12}.$$

The first terms on the right-hand side of (3.8) represent contributions from mixing buoyant water down into the system, while the second terms cover entrainment-induced changes. Note that these contributions are expressed in terms of a finite temperature difference in spite of the fact that the profile is continuous at the mixed layer base. The limit of the original Kraus-Turner (1967) step-type temperature profile is obtained from (3.8) as $h_{12} \to 0$. Then $H_q \to h_1$ and $H_p \to \tfrac{1}{2}h_1$, so that in this case, the system's heat capacity and gravitational depth are always in phase. The present model is seen to provide more flexibility for the relation of H_q and H_p.

Upon insertion of the budgets (3.8), one obtains the dynamical equations of the system

$$\dot{T}_{10} = (F_q(H_1 + H_p) - F_p)/H_q H_1,$$

$$\dot{h}_1 = (F_p - H_p F_q)/[(T_{10} - \theta_2)H_1].$$

These equations are readily integrated, if the bottom temperatures are known as well as the parameterizations of F_p and F_q in terms of the states of the ocean and the atmosphere. However, if these functions are known, it is more convenient to construct

$$R_0(t) = R_0(t_0) + \int_{t_0}^{t} dt' F_q(t')$$

and

$$R_1(t) = R_1(t_0) + \int_{t_0}^{t} dt' F_p(t'),$$

and then solve the transcendental equations (3.7) for T_{10} and h_1. In this way, heat and potential energy will be conserved numerically at low computational expense.

4. Sea-surface temperature-simulation

Appropriate parameterizations for F_p are the main concern of current ML-theories. There exist numerous parameterizations, which are quite satisfactory in the summer season, when there is a pronounced buoyancy-gradient beneath the ML-basis. There are, however, several competing proposals for a mechanism that prevents unrealistically large entrainment rates during winter. Presently available data do not discriminate among these models. In the paper at hand, these problems will be avoided by simply utilizing $R_1(t)$ as derived from the weathership data.

The total heat-flux F_q entering (3.8) is made up by an atmospheric contribution $F_q(t,\mathrm{atm})$ and the advective flux $F_q(t,\mathrm{adv})$. For the present purposes

$$F_q(t,\mathrm{atm}) = F_q(t,\mathrm{ACM}),$$

while $F_q(t,\mathrm{adv})$ has to be estimated. It will be assumed that

$$F_q(t) = F_q(t,\mathrm{ACM}) + F_q(t,\mathrm{adv}) := cF_q(t,\mathrm{ACM}),$$

where the ratio c of the total flux to the atmospheric flux will be considered a constant, which has to be determined from the data at each location. This assumption is purely phenomenological and will be justified a posteriori. In the present context of a 1-D OML-model, this method measures essentially advective effects. It is well-known, however, that even for the coupling of much more sophisticated ocean circulation models with atmospheric circulation models, some procedure of flux adjustment is generally necessary to ensure model compatibility (see for instance Sausen et al., 1988).

To obtain the flux-ratio c from the weathership data the expression

$$R_0(t) := R_0(t_0) + c\int_{t_0}^{t} \mathrm{d}t' F_q(t',\mathrm{ACM}) \tag{4.1}$$

will be fitted in a least square sense to the observed $R_0(t,\mathrm{data})$

$$\int_{\mathrm{Dec}}^{\mathrm{Feb}} \mathrm{d}t[R_0(t,\mathrm{data}) - R_0(t)]^2 = \min. \tag{4.2}$$

(4.1) with the thus-derived optimal values for $R_0(t_0)$ and c will be used in the present SST-simulation.

Since the present SST experiments depend, to a large extent, on a combination of ACM results and observations, both should exhibit a certain degree of consistency. As an ad hoc test, the climatological SST prescribed to the ACM as lower boundary condition are compared to the seasonal cycle of $T_S(t)$ obtained from the data. Fig. 8 shows that the two SST time-series generally match quite well, except for weathership C. Although the phases of the two lines also agree in this case, the ACM boundary condition is 1.3°C warmer than the observations. This indicates that the parameterization of the boundary condition here (in a region of strong horizontal SST-gradients due to the nearby inflow of the Labrador current into the Gulf Stream) overestimates an additive term. Further calculations refer to the observed SST at weathership C, while the distinction between observed and prescribed SST is irrelevant for all other locations.

The results of the SST-simulation for the period from 1 December to 28 February are shown in Fig. 9 (c through m). The uppermost panel displays $R_1(t)$ as obtained from the data. The panel beneath shows $R_0(t)$ as given by the data and the optimal fit of the ACM-fluxes according to (4.2). The next panel shows the mixed layer depth as given by the data and as obtained from the model integration. Finally, the lowest panels give the data $T_s(t)$ in comparison to the model results for the ML-temperature $T_1(t)$.

Initial values for data and model-results do generally not coincide. According to the integration procedure described above, the required intitial conditions are $R_1(t_0)$ and $R_0(t_0)$. While

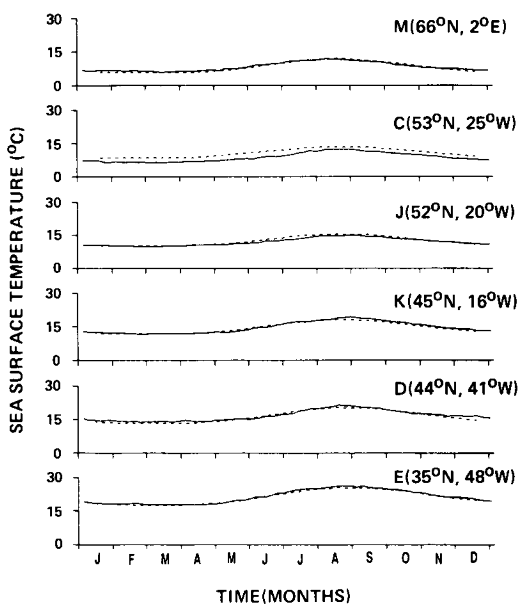

Fig. 8. SST-comparison at weathership locations. Solid line: $T_S(t)$ from weathership data, dotted line: SST boundary condition of UCLA-ACM.

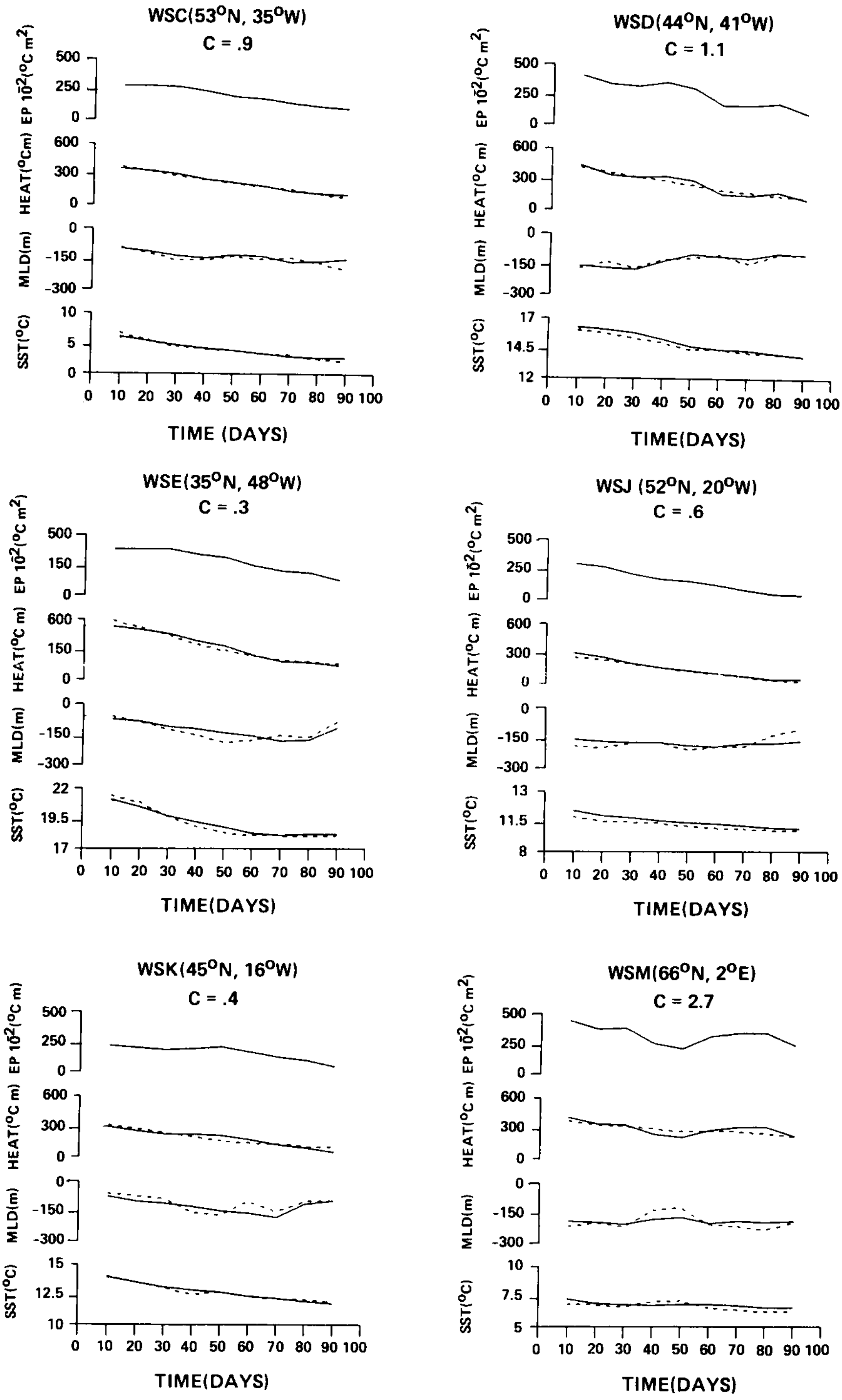

Fig. 9. Results of OML model integration. Dotted lines: model results, solid lines: observations.

$R_1(t_0)$ is uniquely determined by the data, $R_0(t_0)$ is obtained from the least-square fit according to (4.1).

For all 6 locations the model results are in satisfactory agreement with the data, indicating the basic consistency of the heat-fluxes of the UCLA-model with their prescribed boundary conditions. The model SST never differs from the observations more than 0.2°C, while the ML-depth deviates only in extreme cases more than 30 m from the data. As a functional of the SST and the ML-depth, the thermocline scale h_{12} (not shown) exhibits a similar degree of coincidence with the data: discrepancies between model and data are confined to a range of ± 20 m. This indicates that the mixed layer model with this particular forcing works equally well under a wide range of ocean conditions.

Furthermore, Fig. 9 clearly shows that the least-square procedure (4.2), modelling the total heat flux in terms of the ACM-flux is remarkably effective at all locations. This provides an *a posteriori* justification for the assumption (4.1). Basically the success of (4.2) is due to the limitation of the considered time-period to one season. On an annual or even larger time-scale, this very simple procedure can hardly be expected to be appropriate. Nevertheless, the present results imply that the phase of the heat content of the upper ocean during the winter season is dominantly determined by the atmospheric heat flux and not altered by advective contributions.

Numerical values for the flux-ratio c are indicated in the corresponding panels. It may be mentioned that the least-square procedure yields originally numerical values for the parameter $p = c\rho_0 c_p$. Here, $\rho_0 c_p = 4 \cdot 10^6 \mathrm{J/(m^0K)}$ has been chosen for sea water at all locations. Ignoring the extreme value of c at weathership M, it is seen that the numerical values for the flux-ratio separate in two groups. For weatherships E, J, K, the factor is of order 0.5, while it is of order 1 for the chips C and D. A superficial inspection of ocean-maps shows that the first group corresponds to regions of small or no advection, while the second group lies fairly close to the Gulf Stream. Thus, for the first group a factor of order one and for the second group a factor somewhat larger than 1 should be expected. The least square results for the flux ratio c therefore indicate that the heat fluxes calculated by the ACM might be somewhat too large.

5. Conclusion

The coarse version of the UCLA atmospheric circulation model reproduces the climatological features of the global heat flux pattern for the December–February period in qualitative agreement with the data provided by the Esbensen/Kushnir-atlas. The consistency of the model results with respect to the prescribed SST-boundary conditions is tested in 6 OML experiments.

The OML-model generalizes the phenomenological Kraus-Turner concepts to include contributions of the thermocline to the buoyancy-budget of the upper ocean. As suggested by ocean-wide observations, it is assumed that the turbulent velocity field establishes essentially a characteristic temperature profile in the upper ocean. For a given lower boundary condition the Kraus-Turner budgets in conjunction with the self-similarity assumption for the profile provide a closed set of equations for the dynamics of the temperature profile. The implementation of the model does neither require a vertical grid nor a global map of upper ocean parameters, as for instance turbulent transport coefficients.

A combination of ACM results and ocean data is used as forcing for the OML model. The simple assumption that for the entire season the advective heat flux is a constant fraction of the atmospheric flux yields a significant representation of the heat content of the upper ocean at all locations considered. The sea surface temperatures and the mixed-layer depth obtained from the ML-integration are in satisfactory agreement with the observations. Since the SST, prescribed to the UCLA-model as boundary condition, essentially coincide with the observed SST, it is concluded that the model heat fluxes are consistent. This is particularly so, since the OML-model does not contain free parameters, subject to numerical tuning. The experiments indicate however that the ACM exhibits the tendency to overestimate the atmospheric contribution to the total flux. A detailed analysis of quantitative problems in view of coupled ocean-atmosphere models requires a realistic model of advective ocean transports.

6. Acknowledgements

Heat fluxes are courtesy of Professor C. R. Mechoso and the authors would like to thank Professor M. Ghil for helpful discussions. Particular thanks are due to C. Wong for her patient and effective handling of the manuscript. This work was supported by NSF grant No. ATM-86-15424 and ONR grant No. N00014-87-K0331.

REFERENCES

Arakawa, A., 1972. Design of the UCLA General Circulation Model. *Report no. 7*, UCLA, USA.

Arakawa, A. and Schubert, W. 1974. The interaction of a cumulus cloud ensemble with the large-scale environment, Part I. *J. Atmos. Sci. 31*, 674–701.

Deardorff, J. 1972. Parameterization of the planetary boundary layer for use in general circulation models. *Mon. Wea. Rev. 100*, 93–106.

Denman, K. and Miyake, M. 1973. Upper layer modifications at ocean station Papa, Observations and Simulations. *J. Phys. Oceanogr 3*, 185–196.

Esbensen, S. and Kushnir, Y. 1981. The heat budget of the global ocean: An atlas based on estimates from surface marine observations. Climate Research Institute, *Report no. 29*, Oregon State University, Corvallis, OR 97331, USA.

Gill, A. and Turner, J. 1976. A comparison of seasonal thermocline models with observation. *Deep-Sea Res. 23*, 391–401.

Katayama, A. 1972. A simplified scheme for computing radiative transfer in the troposphere. *Report no. 6*, UCLA, USA.

Kraus, E. and Turner J. 1967. A one-dimensional model of the seasonal thermocline. *Tellus 19*, 98–105.

Lemke, P. and Manley, T. 1984. The seasonal variation of the mixed-layer and the pycnocline under polar sea ice. *J. Geo. Res. 89*, 6494–6504.

Maier-Reimer, E., Müller, D., Olbers, D., Willebrand, J. and Hasselmann, K. 1982. An ocean circulation model for climate variability studies. *Rep 104 02612*, MPI für Meteorologie, Hamburg FRG.

Manabe, S., Bryan K. and Spelman, M. 1975. A global ocean-atmosphere climate model. Part I. *J. Phys. Oceanogr. 5*, 3–29.

Müller, D. 1987. Bispectra of sea-surface temperature anomalies. *J. Phys. Oceanogr. 17*, 26–36.

Oort, A. and Von der Haar, T. 1976. On the observed annual cycle in the ocean-atmosphere heat balance over the Northern Hemisphere. *J. Phys. Oceanogr. 6*, 781–800.

Pollard, D., Batteen, M. and Han, Y. 1983. Development of a simple upper ocean and sea ice model, *JPO 13*, 754–786.

Randall, D. 1979. The entraining moist boundary layer. Preprint volume. *4th Sympos. on Turbulence, Diffusion and Air Pollution of the Amer. Meteor. Soc.*, Reno, Nevada, 467–470.

Sausen, R., Barthel, K. and Hasselmann, K. 1988. Coupled ocean-atmosphere models with flux connections. *Climate Dynamics 2*, 175–163.

Schlesinger, M. 1976. A numerical simulation of general circulation of atmospheric ozone. Ph.D. thesis, UCLA, USA.

Simonot, J., 1986. Atlas of the ECMWF energy fluxes and surface stresses (in French). Laboratoire de Météorologie dynamique, Paris, France.

Suarez, M., Arakawa, A. and Randall, D. 1983. The parameterization of the planetary boundary layer in the UCLA general circulation model. Formulation and results. *Mon. Wea. Rev. 111*, 2224–2243.